Preplasma conditions for operation of 10-Hz subjoule femtosecond-laser-pumped nickel-like x-ray lasers

Riccardo Tommasini,* Klaus Eidmann, Tetsuya Kawachi,[†] and Ernst E. Fill

Max-Planck-Institut für Quantenoptik, D-85748 Garching, Germany
(Received 13 October 2003; published 4 June 2004)

We present measurements of electron densities of plasmas with femtosecond (fs) temporal resolution. The plasmas are generated by laser pulses with different intensities at different time delays. Such plasmas are of great interest as preplasmas for transient, collisionally excited x-ray lasers. The laser pulses producing the plasmas are generated by stretching part of a 130-fs laser pulse of the ATLAS titanium-sapphire laser of our institute and focusing this radiation to a line on molybdenum and silver slab targets. The electron density is measured as a function of distance from the target by interferometry using a Wollaston prism. Using an ultrashort probe pulse allows one to obtain data extremely close, about 10 μm, to the target surface. Experimental data are compared with simulations using the MULTI hydrocode. The results allow comparison of the ablation from a hard (Mo) and a soft (Ag) material, optimization of prepulse-main pulse delay times, and selection of the best pump geometry allowing for propagation of the pump and x-ray beams. These points are key elements for the development of a high-repetition-rate soft-x-ray laser.

I. INTRODUCTION

Significant effort is now being made on developing an x-ray laser operating at a repetition rate of 10 Hz. Such a laser would allow the realization of many applications proposed over the years (see, for example, [1]). A possible solution of the problem is based on the transient collisional excitation scheme using ultrashort laser pulses. In this technique a prepulse, with a length of 100 ps or more, is used to generate a plasma with a sufficiently high degree of ionization. After a suitable time delay, a picosecond or femtosecond pulse rapidly heats the medium and drives it into inversion [2–4]. By this method, saturated lasing has been achieved in many nickel-like lasers, such as Sn, Ag, Pd, and Mo, as well as in neonlike lasers at wavelengths ranging from 11 nm to 33 nm [5,6]. However, the major limitation of these x-ray lasers is that they still require a pump energy of several joules, which limits the repetition rates achievable to fewer than 20 shots per hour.

In a variant of the prepulse-induced transient excitation scheme, traveling-wave pumping is realized by applying the heating pulse either at oblique incidence to the target [7] or parallel to it [8], i.e., using longitudinal pumping. The latter scheme recently provided evidence of a low-divergence x-ray laser beam requiring a pump energy of only 150 mJ [4].

Traveling-wave excitation of high gain lasers was indeed proven to be a key issue several years ago when a few seminal papers were published reporting lasing in nitrogen and neon [9] and in the Lyman band [10–12] and the Werner band [13–16] of molecular hydrogen. More recently, a trans-verse pump scheme able to match the velocity of excitation to the velocity of the amplified pulse, employing a step mirror together with oblique incidence, in order to provide a velocity of excitation below the speed of light, was demonstrated with molecular hydrogen as the active medium [17] and is a promising scheme for x-ray lasers [7].

Particularly for longitudinally pumped x-ray lasers, generation of a suitable preplasma is the key issue since in this scheme both the pump beam and the x-ray laser beam must propagate through the preplasma along the target surface. A high electron density gradient will severely deflect the x-ray laser beam and even more so the pump beam because of its longer wavelength.

This paper presents the results of a systematic study of preplasma electron densities using Mo and Ag as the target materials. Both metals are important species for x-ray lasers since their nickel-like ions generate saturated lasers emitting at 18.9 nm (Mo) and 13.9 nm (Ag), respectively. In this research we vary the energy density of the plasma-generating pulse and the time of observation. Since the electron densities amenable to our diagnostic method are well in the range of those of x-ray lasers, we are thus able to investigate the possibilities of generating an optimum preplasma electron density profile.

The basic idea of the experiment is to use interferometry to determine the electron density from measurements of the phase shift suffered by a probe laser beam in a pump-probe experiment [18]. In these kinds of measurements, a limitation in probing electron densities very close to the target arises from motional blurring resulting from a finite duration of the probe pulse. In our experiment, however, application of an ultrashort pulse freezes any motion of the plasma and allows investigation of electron densities extremely close to the target surface.

The aim of the experiment is the measurement of electron densities produced by lasers at very low irradiances, where no experimental data are available to date. Using these data,

---

*Corresponding author. Email address: riccardo.tommasini@mpq.mpg.de

[†]On leave from Advanced Photon Research Center, Japan Atomic Energy Research Institute, Kyoto 619-0215, Japan.
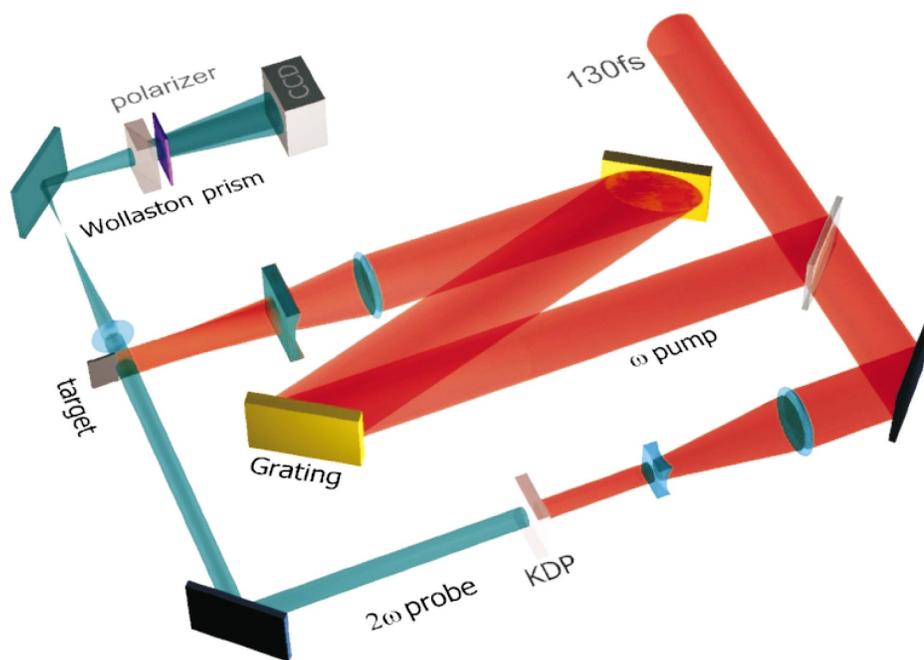
FIG. 1. (Color) Experimental setup for plasma interferometry with fs laser pulses using a Wollaston interferometer. The optical delay line for the probe beam is not shown.

it should be possible to find the optimum preplasma electron density profile and select the best pump geometry, allowing good propagation of the pump beam as well as the x-ray beam for development of a high-repetition-rate soft-x-ray laser.

II. EXPERIMENTAL ARRANGEMENT

Pulses of the ATLAS titanium-sapphire laser at the Max-Planck-Institut für Quantenoptik (Garching, Germany) were used for the pump and the probe (see Fig. 1). In previous experiments, it had been found that femtosecond (fs) pulses did not ablate enough material from the target to generate a sufficiently large preplasma. The pulses generating the preplasma were therefore stretched to a length of 100 ps by means of a grating stretcher. The stretcher consisted of two 1000 1/mm gratings adjusted parallel to each other by means of a He-Ne laser. The stretched pulses, with an energy of 100 mJ at a central wavelength of 790 nm, were focused on the target by a combination of a spherical and a cylindrical lens. In this way, a vertically oriented line focus 4 mm long and 100 μm wide is generated, yielding a maximum intensity of 2.5×10^{11} W/cm^2.

Before the pulse stretcher, a small part of the fs pulse (about 2 mJ) was taken out of the beam by means of a semitransparent mirror. This pulse, the probe pulse, was then frequency-doubled in a potassium dihydrogen phosphate (KDP) crystal and passed through an optical delay line. The temporal interval between the probe pulse and the plasma-generating pulse could be adjusted from 0 ns to 3 ns. The pulse then propagated along the target in a direction transverse to the line focus. In this way, the amount of plasma traversed by the probe pulse was small enough to prevent it from being deflected at electron densities of up to a few 10^{20} cm^{-3}. Radiation at the fundamental frequency, ω, was suppressed using some dielectric mirrors in the optical path

of the probe pulse, i.e., the last two shown in Fig. 1, and a bandpass filter in front of the Wollaston prism.

After traversing the plasma, the pulse was passed through an imaging lens, a Wollaston prism, and a polarizer. The lens generated an image of the plasma at a magnification of 12 on the detector. The polarizer, oriented at 45° to the principal axes of the Wollaston prism, allows interference between ordinary and extraordinary rays. The quartz Wollaston prism, supplied by Fichou, generated an angle of 5 mrad between ordinary and extraordinary beams. A Wollaston interferometer has many advantages, such as simplicity, ease of alignment, and applicability in a wide wavelength range [18]. The interferometer ensures equal optical path lengths for both beams at the central fringe and is thus very well suited to use with fs laser pulses. Note, however, that the interferometer requires a certain amount of spatial coherence across the beam.

The probe beam was detected with a charge-coupled device (CCD) positioned about 1.20 m from the Wollaston. The CCD had a pixel size of 9.3×9.3 μm^2 and a sensitive area of 4.8×4.8 mm^2. The images were stored in digital form and evaluated by computer. Single shots were used for generating the interferograms.

The contrast of the ATLAS Ti:sapphire laser is better than 10^3 and 10^7, on a ps time scale, at ω and 2ω, respectively. Therefore, spurious prepulses or pedestals have no role in our experiment, either for the plasma-generating pulse or for the probe pulse.

III. EVALUATION OF INTERFEROGRAMS

At electron densities N_e much below the critical density N_{crit}, the refractive index n of a plasma can be approximated as

$$n \approx 1 - N_e/2N_{crit} \tag{1}$$

and therefore the fringe shift generated by a homogeneous plasma is given by

$$N_{\text{fringe}} \approx \frac{N_e}{2N_{\text{crit}}} \frac{L}{\lambda}, \qquad (2)$$

where λ is the wavelength of the probe radiation and L is the column length. The critical density of a plasma at the wavelength of the second harmonic of the titanium sapphire laser is 6.9×10^{21} cm^{-3}.

Equation (2) shows that in an interferometric experiment with an expanding plasma, one measures the quantity $N_e L$ and not N_e directly. Knowledge of the column length is therefore required in order to obtain the electron density. An exception to this rule arises when the expanding plasma has cylindrical symmetry with axis normal to the propagation of the probe beam: in this case the problem has a solution given by the Abel inversion. However, in a line-focused plasma, the expansion in directions parallel to the target surface can be neglected at distances comparable to the line-focus width.

A computer algorithm using Fourier-based analysis was employed to extract the accumulated phase shift from the interferograms [19]. The process is well known and can be summarized as heterodyning using the fringe frequency as the carrier and a digital bandpass filter in the Fourier space. The two-dimensional Fourier spectrum of the interference pattern has a central peak at zero frequencies, representing the low-frequency spectral components that arise from the modulation of the background intensity of the interferogram. The two symmetric side lobes carry the same information about the phase values. Using the appropriate bandpass filter in the frequency domain, we can extract one of the side lobes. The modulo-2π phase can thus be calculated by the inverse Fourier transform of the filtered spectrum. Discontinuities of phase values must be correctly removed by the appropriate unwrapping method, i.e., by adding a phase jump of 2π to each discontinuity. The electron density is then calculated on the assumption of a one-dimensional (1D) expansion, which is good given the line-focus geometry for the pump, with L being used as equal to the focal width of 100 μm.

IV. EXPERIMENTAL RESULTS

It was found that a fringe spacing of 96 μm at the CCD plane, corresponding to a fringe spacing of 8 μm at the target plane, was a reasonable compromise to achieve good spatial and phase resolution. Rotating the Wollaston prism and the polarizer allowed the direction of the fringes to be changed. Experiments were performed with the fringes oriented parallel as well as perpendicular to the target surface.

An example of an interferogram obtained with Mo as the target is shown in Fig. 2. For this experiment, the delay time between the pump and probe beams was set at 1 ns. The intensity of the preplasma-generating pulse was 2.5×10^{11} W/cm^2. The figure shows the upper end of the line focus, and thus the upper part is a nonpumped target. Indeed fringes are unaffected, in contrast to the lower part of the figure, where fringes clearly show a shift. The target surface is emphasized with a white line, while the shadow of the target itself is seen to extend into the picture. The high contrast of the fringes even at spatial positions close to the target
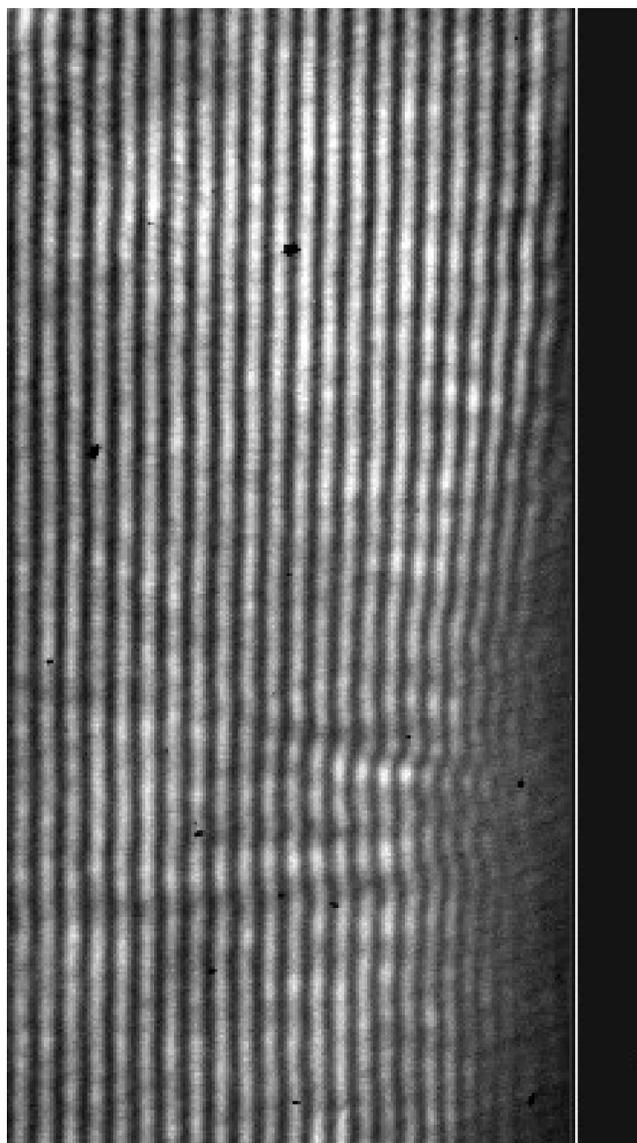

FIG. 2. Interferogram of the upper end of a Mo laser plasma recorded with the second harmonic of a 130 fs titanium-sapphire pulse. The target is visible on the right side of the diagram, while the target surface is emphasized with a white line. The x axis is the one normal to the target surface; the y axis is the one parallel to the target surface. Upper part: no plasma; lower part: with plasma. The delay time is 1 ns. The intensity of the plasma-generating pulse is 2.5×10^{11} W/cm^2.

surface is obvious. The last visible fringe is at about 10 μm from the target surface, in the pumped region.

An evaluation of interferograms with different time delays between the prepulse and probe pulse yields the electron densities shown in Fig. 3. The target material is molybdenum. The prepulse intensity is kept constant at 2.5×10^{11} W/cm^2. The different curves in the diagram show how the plasma fills the space before the target. Evaluation of the fringes is possible down to a distance of about 10 μm from the target surface. At shorter distances, the fringes rapidly disappear owing to beam deflection in the high electron density gradient.
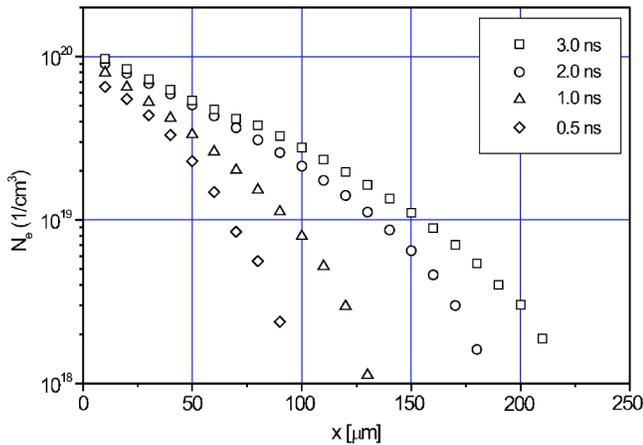
FIG. 3. Electron density for Mo target as a function of distance from target for various time delays. Intensity 2.5×10^{11} W/cm^2.

FIG. 5. Electron density profiles for Ag target as a function of distance from target at various time delays. Intensity 2.5×10^{11} W/cm^2.

Figure 4 shows electron density profiles of Mo targets when the intensity of the pulse is varied. Here the time delay is kept constant at 3 ns. The data illustrate how the higher intensity leads to a greater ablation of target material and also to a higher expansion velocity.

Figures 5 and 6 display time and energy scans for silver as the target material. Comparing these data with those of molybdenum, we note that only a marginally higher electron density is produced. We note further that silver allowed only about five to ten shots at maximum energy on the same target site. With a higher number of shots, indentation of the target was clearly visible in the CCD image and the generated electron density was reduced. For molybdenum, a larger number of shots, about 20, was possible on the same target site.

V. SIMULATIONS

Simulations were carried out by means of the MULTI hydrodynamic code [20]. MULTI is a 1D code which treats radiation by multigroup diffusion. The simulations were performed in planar geometry. The equation of state is taken

from the SESAME library. The radiation emission and absorption coefficients used by the code were calculated by a steady-state non-LTE (local thermodynamic equilibrium) model [21].

Figure 7 shows the electron densities for a Mo target, at an intensity of 2.5×10^{11} W/cm^2 and at delay times of 0.25, 0.5, 1, 2, and 3 ns.

Comparing the simulation results with the experimental data, it appears that the general profiles of the electron density distributions are quite similar. This creates confidence in the other results of the code, e.g., in the predicted electron temperature and the charge state of the ions.

Figures 8 and 9 show the results from MULTI simulations regarding the average ionization stage, Z_i, and the electron temperatures, T_e, for Mo. While experiment and simulations evidenced values of Ne possibly useful for x-ray lasers (10^{19}–10^{20} cm^{-3}) up to a distance of 150 μm from the target and for 2–3 ns as a time delay, the MULTI simulations show that T_e and Z_i are only in a range of 6–9 eV and 3–6, respectively, the latter being much less than a value of 14 for the ionization stage required for nickel-like molybdenum. In
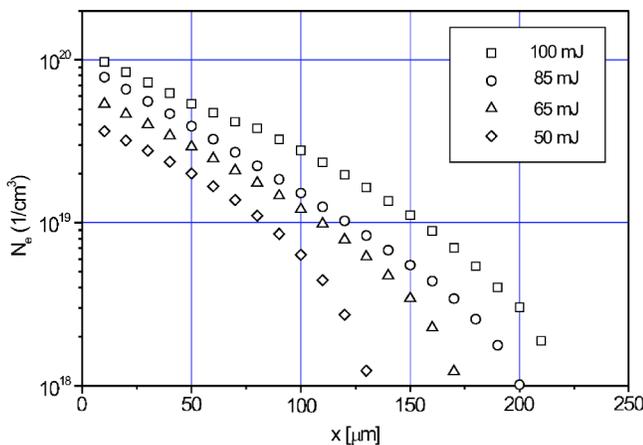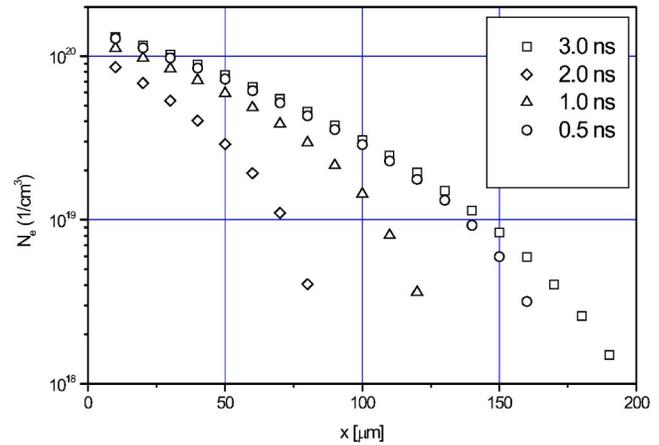

FIG. 4. Electron density profiles for Mo target at different prepulse energies. An energy of 100 mJ corresponds to an intensity of 2.5×10^{11} W/cm^2. Time delay is 3 ns.
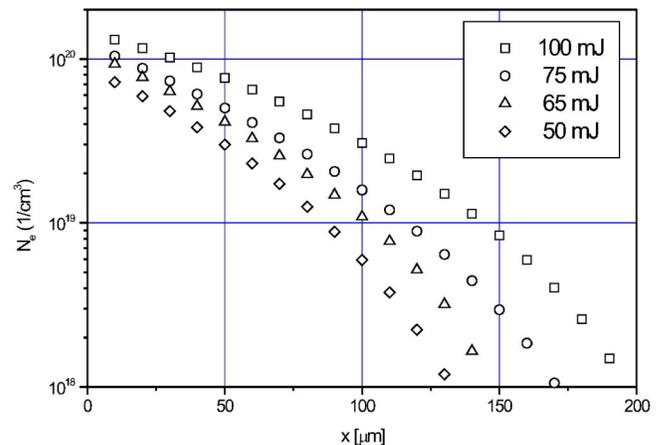

FIG. 6. Electron density profiles for Ag target at different pulse energies. An energy of 100 mJ corresponds to an intensity of 2.5×10^{11} W/cm^2. Time delay is 3 ns.
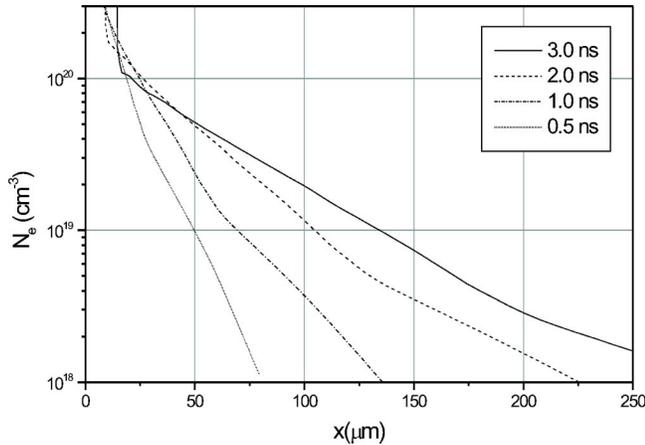
FIG. 7. Simulation of electron density for Mo target by MULTI hydrocode for different time delays. Irradiance is 2.5 $\times 10^{11}$ W/cm^2.

FIG. 9. Simulation of electron ionization stage for Mo target by MULTI hydrocode for different time delays. Irradiance is 2.5 $\times 10^{11}$ W/cm^2.

the case of Ag, the simulation results are very similar to those for Mo so that, for instance, the ionization stage produced by the prepulse appears even farther from what is required for lasing on the nickel-like lines. This means that the heating pulse, in a typical transient collisional scheme, will have to do the rest of the job, i.e., in the case of Mo, raise up Z_i to 14 as well as exciting the nickel-like ions.

VI. CONSIDERATIONS ON THE PUMP GEOMETRIES OF A MO TCE SOFT-X-RAY LASER

In this section, we explicitly refer to the case of Mo, but the same conclusions apply to Ag. Quite generally we note that in a region of electron densities useful for x-ray lasers (around 10^{19}–10^{20} cm^{-3}), the experimental data show electron density gradients of a few 10^{22} cm^{-4}. Fitting an exponential to the data, $N_e = N_0 \exp(-x/x_w)$, and using the analytical formula for the deflection of a beam in an exponential electron density profile, $x = x_0 + x_w \ln(\cosh^2\{(z/2x_w)[N(x_w)/N_{crit}]^{1/2}\})$ [see Eq. (12) of Ref. [22]], where z is the axial coordinate along the plasma column, x_0 is the initial distance
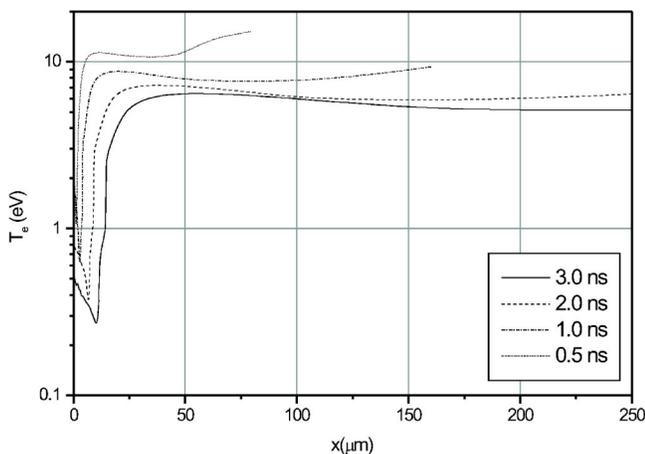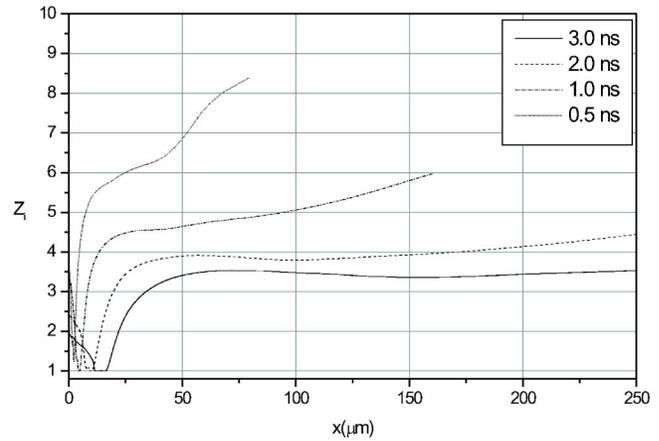

FIG. 8. Simulation of electron temperature for Mo target by MULTI hydrocode for different time delays. Irradiance is 2.5 $\times 10^{11}$ W/cm^2.

from target, and x_w the decay length of the electron density, one can calculate the deflection of a beam propagating through the plasma.

First we notice that the 2ω probe beam even entering at 10 μm from the target is deflected only by 0.5 μm after a 100 μm path, meaning that the data for the electron density close to the target are perfectly reliable.

We now come to the issue of propagation of pulses along the plasma column. At a distance of 50 μm from the target, we derive a deflection of the Mo x-ray laser (18.9 nm) of only about 1 μm after traversing a distance of 4 mm.

However, the pump beam, at a wavelength of 800 nm, is deflected by about 100 μm after traversing a distance of only 1 mm, and even at a wavelength of 400 nm the deflection will be about 30 μm. Note that the deflection increases nonlinearly with the distance traversed. Even worse, since the trajectory of the x rays is almost unaffected by the plasma, the longitudinal pump beam and the x-ray beam to be amplified will follow completely different paths.

Figure 10 shows the calculated ray trajectory, from the experimental measurements of the electron density of Mo plasma, for a longitudinal pump beam, 800 nm wavelength, starting at a distance of 50 μm from target. The beam is severely refracted out of the high-density regions, while the x-ray beam propagates almost straight. Note that the pump beam also undergoes focusing due to the electron-density gradient.

These results show that special measures have to be taken to avoid refraction of the pump beam out of the high-density region, and that a longitudinal pump always gives rise to insufficient coupling between the heating pulse and the x rays. With this in mind, a traveling-wave transverse-pump geometry [17] seems, in principle, to be a far better solution.

On the other hand, we notice that starting from about 0.6 mm as a target length, the trajectory of the pump beam is linear to good approximation. If we consider a pump beam strong enough to produce the lasing conditions at the densities measured up to and beyond a distance of 250 μm from the target, then an x-ray beam can be produced and amplified in the last, and longer, linear segment of the plasma column. This beam will emerge from the plasma at an angle of about
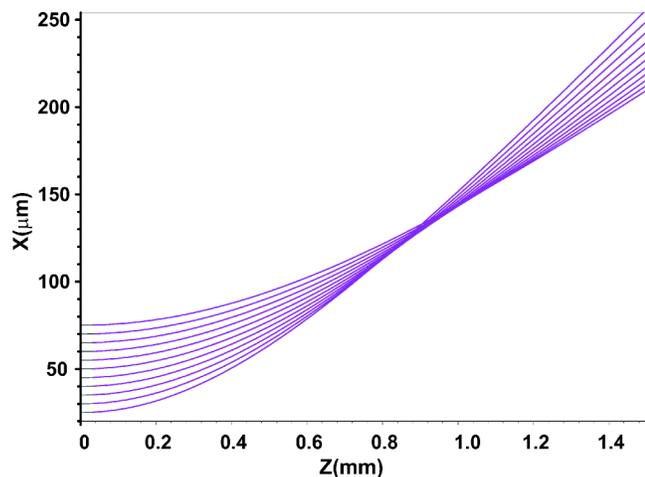
FIG. 10. Calculated ray trajectories for an 800-nm wavelength longitudinal pump beam starting at a distance of 50 μm from the target. The beam is severely refracted out of the high-density regions. It also undergoes focusing due to the electron-density gradient.

10° with respect to the target surface, as can be easily calculated from the Eq. (7) of Ref. [22], $\phi_\infty = \sqrt{N_0/N_{\text{crit}}} \exp(-x_0/2x_w)$, if the longitudinal pump beam enters the plasma at 50 μm from the surface, or 7° if the longitudinal pump beam enters the plasma at 100 μm from the surface. These considerations add some hints to the recent results obtained by Ozaki *et al.* [4], using a longitudinal pump for TCE in nickel-like Mo.

Note that Fig. 10 has a second interpretation: with the z axis reversed, it gives the best incidence angle for the transverse pump in oblique incidence geometry, i.e., the entrance angle maximizing the arclength that the pump beam will travel with a direction parallel to the target, or, in other words, the angle resulting in the maximum distance traveled in the closest-approach electron density region. Again these angles are 12°, 10°, or 7° if the closest-approach distance from the target surface is 25 μm, 50 μm, or 100 μm, respectively.

VII. CONCLUSION

Using frequency-doubled pulses from a femtosecond titanium-sapphire laser, we were able to measure electron density profiles generated by a 100-ns prepulse. The prepulse was a stretched fs pulse with a wavelength of 790 nm. The data allow one to determine the optimum time delay, be-tween the prepulse and the main pulse, at which the electron density gradient is low and the electron density itself is still high enough in a sufficiently extended region around the target. We also note significant differences in the amount of ablated material in going from Mo to the softer Ag target, the latter allowing much fewer shots to obtain good enough conditions for generating a suitable preplasma.

It is interesting to compare our results with those obtained using a nickel-like palladium soft-x-ray laser as a probe [23]. The critical electron density for the Pd x-ray laser ($\lambda = 14.7$ nm) is 5.1×10^{24} cm^{-3}. Nevertheless, the measurements extend to an electron density of only $< 1.2 \times 10^{20}$ cm^{-3} limited by plasma self-emission and motional blurring due to the pulse duration of 6 ps. Our experiments using 400-nm light extend up to similar electron densities, in spite of a critical electron density of only 6.9×10^{21} cm^{-3}. This is due to the fact that for fs pulses, motional blurring plays no role and, in addition, in the visible spectral region, self-emission of the plasma is very low.

As a general feature of the preplasmas generated, we note that the electron density gradients easily allow propagation of a soft-x-ray laser beam over a distance of several mm. Furthermore, gain guiding [24] can alleviate the refraction problem. However, propagation of the pump laser is severely affected by refraction. Special measures, such as a pedestal in the pump beam, are reported to generate a dip in the electron density distribution [4], but it is not clear how this can be achieved along a straight path parallel to the target surface. Further investigations involving interferometry with an applied pump pulse are needed in order to clarify this aspect.

In any case, the traveling-wave transverse pump appears to be the most straightforward way to avoid any refraction problems in the pump beam and also allows the velocity of excitation to be matched to the velocity of the amplified pulse [17]. The best oblique-incidence angles have been calculated according to the experimental measurements of electron densities for Mo.

[1] R. C. Elton, *X-RAY Lasers* (Academic, San Diego, 1990).
[2] P. V. Nickles, V. N. Shlyaptsev, M. Kalachnikov, M. Schnurer, I. Will, and W. Sandner, Phys. Rev. Lett. **78**, 2748 (1997).
[3] J. Dunn, A. L. Osterheld, Y. L. Li, J. Nilsen, and V. N. Shlyaptsev, IEEE J. Sel. Top. Quantum Electron. **5**, 1441 (1999).
[4] T. Ozaki, R. A. Ganeev, A. Ishizawa, T. Kanai, and H. Kuroda, Phys. Rev. Lett. **89**, 3902 (2002).
[5] J. Dunn, A. L. Osterheld, R. Shepherd, W. E. White, V. N. Shlyaptsev, and R. E. Stewart, Phys. Rev. Lett. **80**, 2825 (1998).
[6] J. Dunn, J. Nilsen, A. L. Osterheld, Y. Li, and V. N. Shlyaptsev, Opt. Lett. **24**, 101 (1999).

[7] R. Tommasini, J. Nilsen, and E. Fill, in *Soft X-Ray Lasers and Applications IV*, edited by E. Fill and J. J. Rocca (SPIE, San Diego, CA, 2001) [Proc. SPIE **4505**, 85 (2001)].

[8] R. Li and Z. Xu, J. Phys. IV **11**, 27 (2001).

[9] J. D. Shipman, Appl. Phys. Lett. **10**, 3 (1967).

[10] R. T. Hodgson, Phys. Rev. Lett. **25**, 494 (1970).

[11] R. W. Waynant, J. D. J. Shipman, R. C. Elton, and A. W. Ali, Appl. Phys. Lett. **17**, 383 (1970).

[12] R. T. Hodgson and R. W. Dreyfus, Phys. Lett. **38**, 213 (1972).

[13] R. T. Hodgson and R. Dreyfus, Phys. Rev. Lett. **28**, 536 (1972).

[14] R. W. Waynant, IEEE J. Quantum Electron. 8 (1972).

[15] R. W. Waynant, Phys. Rev. Lett. **28**, 533 (1972).

[16] R. W. Dreyfus and R. T. Hodgson, Phys. Rev. A **9**, 2635 (1974).

[17] R. Tommasini and E. Fill, Opt. Lett. **26**, 689 (2001).

[18] R. Benattar, C. Popovics, and R. Sigel, Rev. Sci. Instrum. **50**, 1583 (1979).

[19] M. Kalal and B. Luther-Davies, J. Appl. Phys. **64**, 3845 (1988).

[20] R. Ramis, R. Schmalz, and J. Meyer-Ter-Vehn, Comput. Phys. Commun. **49**, 475 (1988).

[21] K. Eidmann, Laser Part. Beams **12**, 223 (1994).

[22] E. E. Fill, J. Opt. Soc. Am. B **14**, 1505 (1997).

[23] J. Dunn, *et al.*, in *Soft X-ray Lasers and Applications IV*, edited by E. Fill and J. Rocca (SPIE, San Diego, CA, 2001) [Proc. SPIE **4505**, 62 (2001)].

[24] E. E. Fill, Opt. Commun. **67**, 441 (1988).